

MIT Open Access Articles

*Clausius–Clapeyron Scaling of Peak CAPE in
Continental Convective Storm Environments*

The MIT Faculty has made this article openly available. **Please share** how this access benefits you. Your story matters.

Citation: Agard, Vince, and Kerry Emanuel. "Clausius–Clapeyron Scaling of Peak CAPE in Continental Convective Storm Environments." *Journal of the Atmospheric Sciences* 74, 9 (September 2017): 3043–3054 © 2017 American Meteorological Society

As Published: <http://dx.doi.org/10.1175/JAS-D-16-0352.1>

Publisher: American Meteorological Society

Persistent URL: <http://hdl.handle.net/1721.1/114581>

Version: Final published version: final published article, as it appeared in a journal, conference proceedings, or other formally published context

Terms of Use: Article is made available in accordance with the publisher's policy and may be subject to US copyright law. Please refer to the publisher's site for terms of use.



Clausius–Clapeyron Scaling of Peak CAPE in Continental Convective Storm Environments

VINCE AGARD AND KERRY EMANUEL

Massachusetts Institute of Technology, Cambridge, Massachusetts

(Manuscript received 4 December 2016, in final form 19 June 2017)

ABSTRACT

A thermodynamic constraint on convective available potential energy (CAPE) in continental environments is established using an idealized one-dimensional model. This theoretical model simplifies the synoptic-scale preconditioning framework for continental severe convection by considering a dry adiabatic column that comes into contact with a moist land surface. A system of equations is derived to describe the evolution of the ensuing surface boundary layer. From these, the maximum value of transient CAPE in the column can be found for any particular combination of surface temperature and moisture. It is demonstrated that, for a given range of surface temperatures, the value of peak CAPE scales with the Clausius–Clapeyron relation.


1. Introduction

Constraining the intensity of severe local storms in continental environments presents a major problem at the intersection of convective meteorology and climate. While continental convective storms can be among the most severe on Earth (Zipser et al. 2006), the problem of how such storms may vary as a function of climate has only recently begun to be addressed substantially (Brooks 2013; Tippett et al. 2015).

Convective storms present a unique challenge in that their spatial extent is too small for them to be resolved by general circulation models. This difficulty is exacerbated in continental convective environments, where, unlike for oceanic convection, the atmosphere cannot be considered to be in radiative–convective equilibrium. Therefore, climate research on these severe local storms often focuses on the environments in which severe local storms are formed. Convective available potential energy (CAPE) and deep-layer vertical wind shear are two important parameters that, when considered in tandem, provide a metric for the propensity of a given environment to support severe convection (Brooks 2009; Grams et al. 2012). Both CAPE and shear are necessary

(although not sufficient) ingredients for severe convection over land, and their respective climatologies are important for determining the climatology of severe local storms. Here, we focus solely on constraining peak values of CAPE over land. We do not make any determinations about vertical wind shear as a function of climate, and therefore this study does not explicitly forecast changes in severe local storm climatology.

However, CAPE by itself still offers a significant environmental constraint on severe storms. Higher values of CAPE theoretically correspond to more intense storms (Weisman and Klemp 1982; Holton 2004), as CAPE provides an upper bound for the theoretical maximum updraft speed. Higher updraft speeds can in turn support larger hydrometeors or ground-level winds associated with a given storm. High CAPE is often associated with especially severe types of continental convection, such as supercells (Emanuel 1994; Rasmussen and Blanchard 1998; Bluestein 2007). Recently, several authors have studied the behavior of continental CAPE in projected future climates using general circulation models. Trapp et al. (2007) and Del Genio et al. (2007) predict increases in CAPE in the eastern half of the United States and over land in general, respectively, under increased greenhouse radiative forcing. Diffenbaugh et al. (2013) and Seeley and Romps (2015) find evidence of CAPE driving an increase in favorable conditions for U.S. severe convection in data from the the Coupled Model Intercomparison Project, phase 5, suite of climate models.

 Denotes content that is immediately available upon publication as open access.

Corresponding author: Vince Agard, jva@mit.edu

Other studies achieve similar conclusions using dynamical downscaling of climate models (Gensini and Mote 2015) and numerical pseudo-global-warming experiments (Trapp and Hoogewind 2016).

Yet, despite a growing consensus from modeling studies that continental CAPE should increase with increased greenhouse gas forcing, a quantitative theory underpinning this change remains elusive. In general, one would expect warming scenarios in which temperature and moisture increase close to the surface to produce increased atmospheric instability. But can we say something more specific about the particular paradigm of instability generation that supports severe convection over land? Currently, a theoretical constraint on even the order of magnitude of CAPE in such environments does not exist. For instance, why should CAPE be 2000 J kg^{-1} , and not 200 or $20\,000 \text{ J kg}^{-1}$?

While other studies (Parodi and Emanuel 2009; Sobel and Camargo 2011; Romps 2011; Singh and O’Gorman 2013) have derived scalings to constrain equilibrium energy scales for convection in the tropics, the highly transient nature of CAPE in continental environments precludes the use of a quasi-equilibrium framework for its study. Rather than quasi equilibrium, the continental convection paradigm involves the time-dependent buildup and storage of potential energy in conditionally unstable profiles. It is the peak values of transient CAPE, rather than the time-averaged background levels, that are therefore relevant to the severe storm environments in which we are interested. Therefore, we develop a simple, idealized initial value problem encompassing a typical condition in which severe local storms might form in continental environments.

2. Idealized model

The scenario being modeled is one that is canonically associated with favorable severe weather environments over North America: The southwestern high desert gives rise to a hot, dry air mass that is advected eastward by the mean flow aloft. Under certain synoptic conditions, upon moving east of the Rocky Mountains, this air mass is superimposed above cooler, moister air near the surface in the Great Plains and Midwest (Emanuel 1994; Schultz et al. 2014). These regions are home to the continent’s most frequent occurrences of extreme peak CAPE (Brooks et al. 2003b), as the dry air mass acts as an inhibitive cap, allowing CAPE to rise as energy builds at the surface. It should be noted that the relative motion of the “dry” and “moist” air masses aloft and near the surface, respectively, often also provides the requisite shear for supporting severe local storms.

With an inhibitive cap in place aloft, CAPE can be generated by one of three mechanisms (Emanuel 1994).

First, air in the free troposphere can be radiatively cooled, thereby increasing instability for parcels lifted from near the surface. A second possible mechanism for CAPE buildup in this scenario is the low-level advection of high-entropy air from outside the column, causing an increase in instability by supplying increased heat and moisture to the boundary layer from which parcels might be lifted. Finally, CAPE can be generated by the diabatic heating of near-surface air from below, as heat and moisture (to the extent to which moisture is available) are fluxed from the land surface into the boundary layer in response to diurnal solar forcing. In general, the differential advection pathway and the diabatic heating pathway are thought to be the most important in generating CAPE in severe storm environments such as those in the Great Plains, with the former being more important earlier in the spring season when synoptic forcing is greater (Brooks et al. 2003a).

This model examines the diabatic heating pathway in which low-level moisture in the boundary layer below the elevated inhibitive cap is generated in situ through the flux of latent heat from the land surface. In the sense that the model generates transient peaks of CAPE in the absence of external low-level advection, we thereby demonstrate that the placement of dry air over a moist land surface in the presence of diabatic heating is sufficient for providing instability to continental severe storm environments.

The synoptic-scale circumstances outlined above can be simply and ideally modeled by considering a one-dimensional problem in which a dry adiabatic column is placed in contact with a moist surface. As in the real-world case of dry desert air placed above a moister vegetated surface, surface latent heat flux gives rise to a moist surface boundary layer that expands with time, given some radiative input to the surface.

The model consists of a single column of atmosphere placed atop a zero-heat capacity land surface. To study the simplest possible case, we begin with an atmosphere that has zero water vapor everywhere. The column is assumed to follow a dry adiabatic temperature profile throughout its entire depth, with a near-surface air temperature of T_0 . This preinitial condition is shown schematically in Fig. 1a (an example of the temperature profile created is shown in Fig. 7a).

Then, at time $t=0$, a cooler, moister surface is instantaneously introduced. To accommodate the new lower boundary condition, a surface boundary layer with some initial height h_0 is created, as shown in Fig. 1b. The boundary layer is assumed to have a nonzero specific humidity that is constant with height, and a temperature profile that follows a dry adiabat (but at a cooler temperature than the that of the preinitial dry column). It is

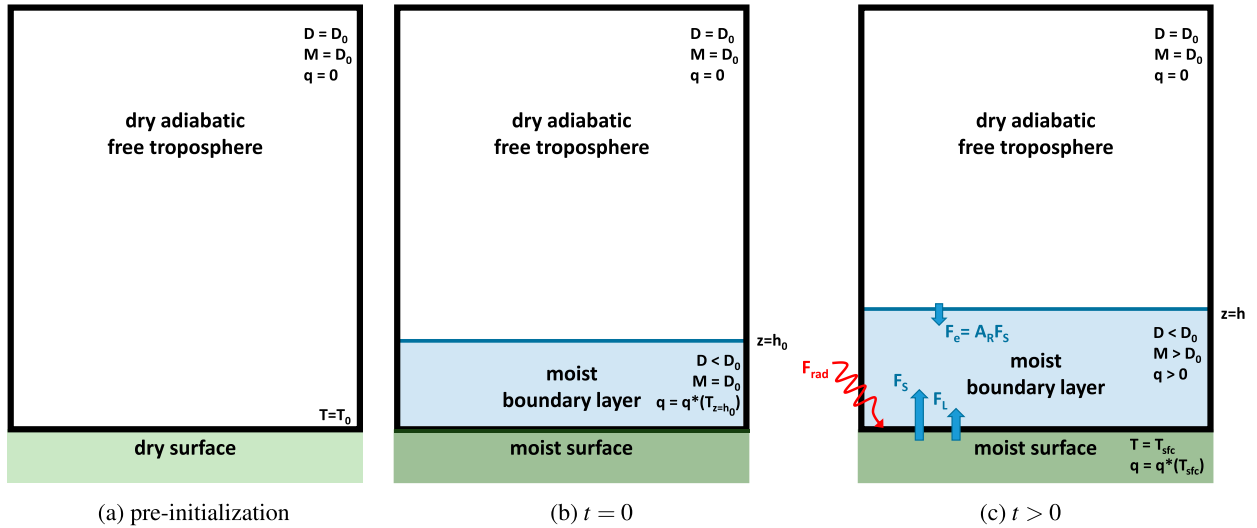


FIG. 1. Schematic of the single-column idealized model (a) before introduction of the moist surface and boundary layer, (b) at the initial time, and (c) during its evolution. Indicated on each diagram are the dry static energy D , moist static energy M , temperature T , and specific humidity q of each part of the system.

assumed (for a perfectly moist surface) that the air at $z = h_0$ has cooled to its wet-bulb temperature, such that saturation is achieved exactly at the top of the boundary layer. For less moist surfaces, we assume that the air at $z = h_0$ achieves a relative humidity equal to the evaporative fraction of the surface. The column above $z = h_0$ (henceforth the “free troposphere”) remains unperturbed, and retains its initial dry adiabatic temperature profile (an example of this is shown in Fig. 7b).

At time $t > 0$, the system is forced with a constant net radiative flux F_{rad} into the surface. Since the land surface has zero heat capacity, we require the radiative input to be exactly balanced by a sensible heat flux F_S and a latent heat flux F_L from the surface into the boundary layer. As time evolves, the boundary layer expands upward, entraining dry air from above as it does so. There is an associated entrainment heat flux F_e owing to the discontinuous jump in temperature between the boundary layer and free troposphere. This configuration is illustrated in Fig. 1c.

It is assumed that the depth of the surface boundary layer is greater than the Monin and Obukhov (1954) length, so that the growth of the boundary layer is thermodynamically, rather than mechanically driven. We therefore assume the entrainment flux at the top of the boundary layer to be proportional by a constant A_R to the surface sensible heat flux, as in Lilly (1968):

$$F_e = \rho(D_0 - D)w_e = A_R F_S, \quad (1)$$

where w_e is the entrainment velocity, a measure of the turbulent entrainment into the boundary layer of

quiescent air from above, and ρ is a reference density of air. A typical value of A_R is 0.2.

The evolution of the system is modeled in terms of the dry and moist static energies of the boundary layer and free troposphere. Since the free troposphere contains no moisture and retains the dry adiabatic temperature profile of the preinitial column for all time, its dry and moist static energy are both equal to the constant

$$D_0 = c_p T_0, \quad (2)$$

where c_p is the specific heat capacity of dry air. Meanwhile, since the boundary layer has a constant vertical profile of water vapor and a dry adiabatic temperature profile, its dry static energy D and moist static energy M are both constant in height (but not in time). We assume that the initial moistening of the boundary layer is done in a way that conserves moist static energy, so at $t = 0$, $M = D_0$. However, since the boundary layer is therefore cooled during the initial moistening, it has an initial dry static energy $D < D_0$ at $t = 0$, with a discontinuity in dry static energy across the interface between the boundary layer and the free troposphere. Therefore, at the beginning of the initial value problem, there is a deficit of dry static energy in the boundary layer with respect to the free troposphere. This deficit in dry static energy can be thought of as a measure of the inhibitive cap arising from the temperature inversion at the interface with the free troposphere.

As time evolves, heating of the boundary layer by F_S and F_e causes D to increase, thereby decreasing the deficit in dry static energy. The decreasing dry static energy deficit represents the erosion of convective

inhibition by diabatic heating. Consequently, when the dry static energy deficit goes to zero, the cap is eliminated and convection can be thermodynamically triggered: this represents the end of the problem we address here.

Concurrently, the fluxes of heat and moisture from the land surface into the boundary layer cause M to initially increase, thereby creating a surplus in moist static energy in the boundary layer with respect to the free troposphere. This moist static energy surplus will serve as a proxy for the thermodynamic instability of the column.

The evolutions of D , M , and the boundary layer height h with time t are described by a set of ordinary differential equations:

$$\rho h \frac{dD}{dt} = F_S + \rho w_e (D_0 - D), \quad (3)$$

$$\rho h \frac{dM}{dt} = F_{\text{rad}} + \rho w_e (D_0 - M), \quad (4)$$

$$\frac{dh}{dt} = w_e, \quad (5)$$

$$F_S = \rho C_T v_{\text{sfc}} (c_p T_{\text{sfc}} - D), \quad (6)$$

$$F_L = \alpha \rho C_T v_{\text{sfc}} [L_v q^*(T_{\text{sfc}}) - M + D], \quad \text{and} \quad (7)$$

$$F_S + F_L = F_{\text{rad}}. \quad (8)$$

Here, the rate of change of the boundary layer height h is set equal to the entrainment velocity w_e , as defined by (1). This velocity scale therefore governs both the growth of the boundary layer and the dilution of its dry and moist static energies. We have also introduced the nondimensional coefficient α to modify the availability of surface moisture for evaporation. This evaporative fraction parameter holds a fractional value between 0 and 1, with those limits effectively representing a totally dry surface, and an (zero heat capacity) ocean surface, respectively. The bulk aerodynamic flux formulas also include the parameter v_{sfc} , an assumed background wind speed for surface fluxes, and the time-dependent temperature of the land surface T_{sfc} . Finally, L_v is the latent heat of vaporization of water, and C_T is the nondimensional aerodynamic flux coefficient.

At $t=0$, the initial conditions of the system are given by

$$D = D_0 - \Delta D_{\text{init}}, \quad (9)$$

$$M = D_0, \quad \text{and} \quad (10)$$

$$h = h_0, \quad (11)$$

where ΔD_{init} is calculated from the assumption of fractional saturation at the top of the initial boundary layer, according to

$$\Delta D_{\text{init}} = c_p (T_0 - T_{b_{\text{init}}}), \quad (12)$$

$$T_{b_{\text{init}}} = T_w + gh_0, \quad \text{and} \quad (13)$$

$$c_p T_w + \alpha L_v q^*(T_w) = c_p (T_0 - gh_0), \quad (14)$$

where $T_{b_{\text{init}}}$ is the near-surface air temperature in the initial boundary layer, and T_w is the temperature at the top of the initial boundary layer; T_w is the temperature achieved by cooling the preinitial air at $z=h_0$ to the point at which its relative humidity is equal to α , while conserving moist static energy.

The time-dependent variables are nondimensionalized according to

$$\delta \equiv \frac{D_0 - D}{D_0}, \quad (15)$$

$$\mu \equiv \frac{M - D_0}{D_0}, \quad (16)$$

$$\eta \equiv \frac{h}{h_0}, \quad (17)$$

$$\tau \equiv \frac{C_T v_{\text{sfc}} t}{h_0}, \quad (18)$$

$$\delta_s \equiv \frac{c_p T_{\text{sfc}}}{D_0}, \quad \text{and} \quad (19)$$

$$\mu_s \equiv \frac{c_p T_{\text{sfc}} + L_v q^*(T_{\text{sfc}})}{D_0}, \quad (20)$$

where δ , μ , η , and τ represent the dry static energy deficit, moist static energy surplus, boundary layer height, and time, respectively. The dry and moist static energies of the land surface are represented by δ_s and μ_s . All variables are defined to be positive-definite.

Additionally, we define the nondimensional constant

$$\Phi \equiv \frac{F_{\text{rad}}}{\rho C_T v_{\text{sfc}} D_0} \quad (21)$$

to represent the net radiative surface input.

Applying the normalizations in (15)–(21) to (3)–(8) yields the following nondimensional system of equations:

$$\frac{d\delta}{d\tau} = -\frac{1 + A_R}{\eta} (\delta_s + \delta - 1), \quad (22)$$

$$\frac{d\mu}{d\tau} = \frac{\Phi}{\eta} - \frac{\mu A_R}{\eta \delta} (\delta_s + \delta - 1), \quad (23)$$

$$\frac{d\eta}{d\tau} = \frac{A_R}{\delta} (\delta_s + \delta - 1), \quad \text{and} \quad (24)$$

$$(1 - \alpha)(\delta + \delta_s) + \alpha(\mu_s - \mu) - 1 = \Phi. \quad (25)$$

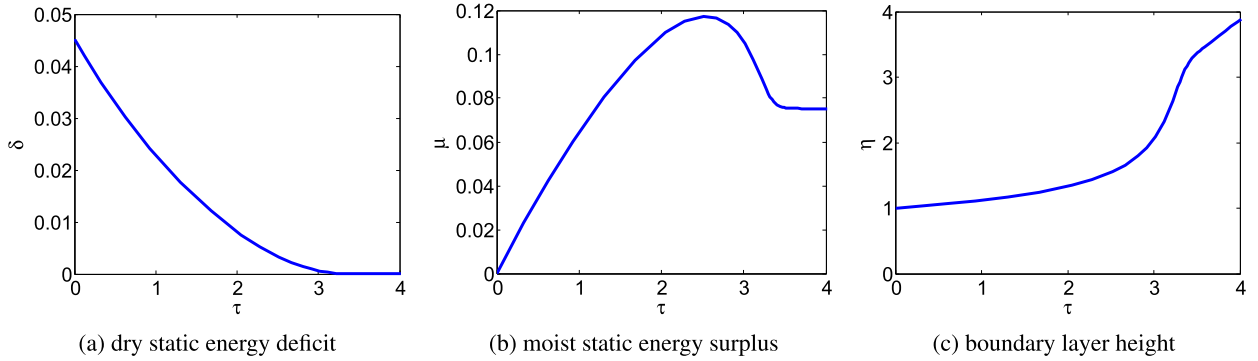


FIG. 2. Numerically integrated time series of (a) δ , (b) μ , and (c) η for $T_0 = 305 \text{ K}$, $\alpha = 0.5$, $h_0 = 100 \text{ m}$, $v_{\text{sfc}} = 5 \text{ m s}^{-1}$, and $F_{\text{rad}} = 200 \text{ W m}^{-2}$.

This system is partially analytically integrated to arrive at a system of three diagnostic equations and one time-dependent ODE:

$$\delta = \delta_{\text{init}} \eta^{-(1+A_R)/A_R}, \tag{26}$$

$$\mu = \frac{\Phi}{\eta} \tau, \tag{27}$$

$$\frac{d\eta}{d\tau} = \frac{A_R}{\delta} (\delta_s + \delta - 1), \text{ and} \tag{28}$$

$$(1 - \alpha)(\delta + \delta_s) + \alpha(\mu_s - \mu) - 1 = \Phi. \tag{29}$$

Note that, while these four equations contain five unknown variables, both δ_s and μ_s are functions of the surface temperature T_{sfc} , as described by (19) and (20).

At time $\tau = 0$, the nondimensional initial conditions are given by

$$\delta = \delta_{\text{init}}, \tag{30}$$

$$\mu = 0, \text{ and} \tag{31}$$

$$\eta = 1. \tag{32}$$

The system is integrated numerically to achieve time series of δ , μ , and η . The integration ends when $\delta = 0$, since at that time the temperature inversion has been erased, and convection is therefore thermodynamically permitted.

3. Results

Solutions to (26)–(29) fall into three distinct categories, depending on the choice of parameters T_0 , α , v_{sfc} , and F_{rad} . Figure 2 shows an example solution belonging to the intermediate category. However, this solution exhibits characteristics common to each category of solutions:

After $\tau = 0$, δ decreases monotonically with time as heat is fluxed into the boundary layer from the surface

and entrained from above, causing the temperature of the boundary layer to approach that of the free troposphere. Likewise, the height of the boundary layer increases monotonically with time, as the entrainment flux from the free troposphere remains positive. While the boundary layer initially grows relatively slowly, the growth rate increases substantially toward the end of the problem as the dry static energy deficit is eroded and the temperature jump across the interface with the free troposphere becomes small.

The rapid expansion of the boundary layer at later times results in nonmonotonic behavior of μ . While μ initially increases as a result of the flux of moist static energy from the moist surface into the boundary layer, the rapid entrainment of dry air from the free troposphere at later times causes the moist static energy of the boundary layer to decrease. Consequently, the moist static energy surplus reaches a maximum some time before the end of the problem. This transient peak in μ corresponds to a transient peak in CAPE.

After its peak is reached, the behavior of the μ time series depends on the problem’s location in parameter space, as shown in Fig. 3. Keeping other parameters constant, the time evolution of the moist static energy surplus falls into one of three regimes, depending on the temperature of the initial dry profile.

At low temperature, the moist static energy of the boundary layer subsides to that of the free troposphere ($\mu \rightarrow 0$) as the temperature of the boundary layer approaches that of the free troposphere ($\delta \rightarrow 0$). In this regime, the convective instability of the column is completely eliminated at the same time that its convective inhibition goes to zero. Thermodynamically triggered convection is therefore impossible. However, the thermodynamic instability of the column does reach a transient peak shortly before the inhibitive cap is exhausted, at which time convection could be triggered by modest dynamic uplift.

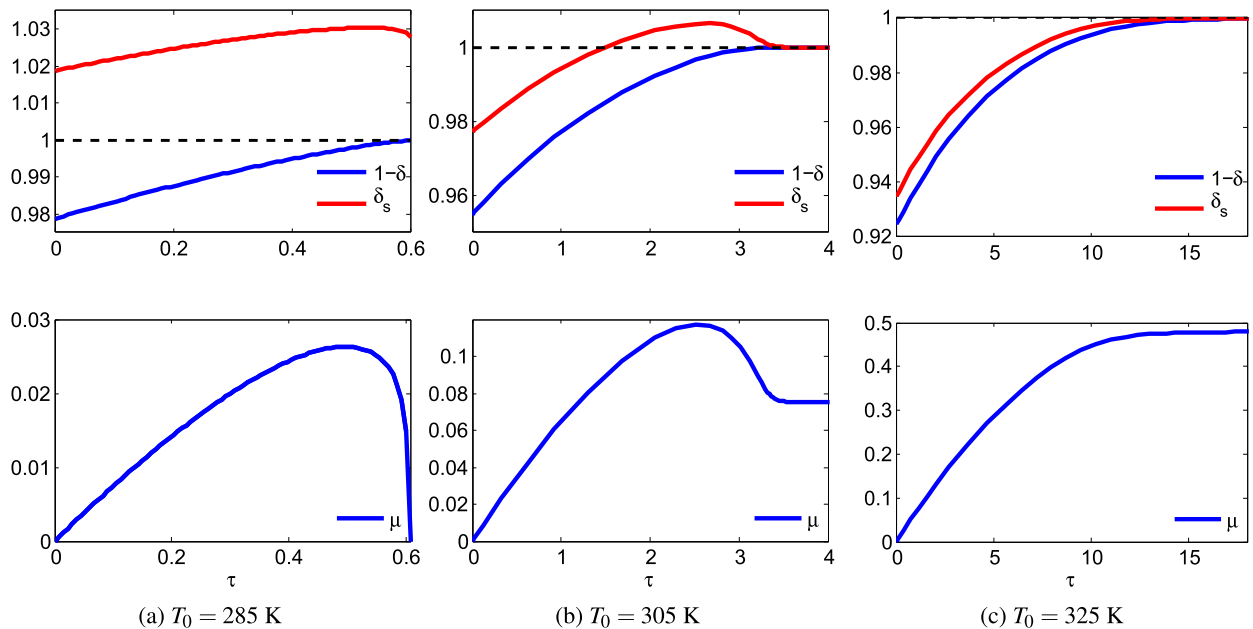


FIG. 3. (top) Time evolution of boundary layer dry static energy (solid blue line) and surface dry static energy (solid red line) for three different values of T_0 , with $\alpha = 0.5$, $h_0 = 100$ m, $v_{\text{sfc}} = 5$ m s $^{-1}$, and $F_{\text{rad}} = 200$ W m $^{-2}$. Boundary layer dry static energy is plotted as $1 - \delta$ to provide a nondimensionalized measure of near-surface air temperature. The dashed black line at $\delta = 1$ represents the level at which temperature is equal to T_0 . (bottom) Time evolution of the moist static energy surplus corresponding to each case. Panels represent the (a) peak, (b) intermediate, and (c) asymptotic regimes.

At warmer temperatures, the system enters an intermediate regime, in which μ reaches a transient peak before relaxing to a finite positive value. The value that μ attains in its long time limit is dictated by the initial temperature of the dry adiabatic profile T_0 . In this regime, thermodynamically triggered convection is possible, since a finite amount of instability remains after the dry static energy deficit is removed. Still, a transient peak in μ is reached while δ is nonzero in this regime.

Finally, at the warmest temperatures, the moist static energy surplus has no transient maximum at all. Instead, the maximum value of μ is approached asymptotically as δ goes to zero as time goes to infinity. In this regime, the maximum value of the moist static energy surplus is identical to its long time limit.

In all three regimes, two of the three requirements for preconditioning the environment for deep convection (as outlined in Doswell et al. 1996) are met: The environmental temperature profile is conditionally unstable, and the boundary layer contains sufficient moisture such that lifted parcels will become saturated and positively buoyant if they enter the free troposphere. The final requirement, which applies in all three regimes when μ is maximized before δ goes to zero, is that some process provides dynamical lift for parcels to reach their level of free convection. The

question of how and when this trigger is provided is outside the scope of this study, but we can still attain information about the magnitude of the transient peak in conditional instability.

In both the intermediate regime and the fully asymptotic regime, the long time limit of the dimensional moist static energy surplus is given by

$$\lim_{t \rightarrow \infty} M - D_0 = L_v q^*(T_0) - \frac{F_{\text{rad}}}{\alpha \rho C_T v_{\text{sfc}}}, \quad (33)$$

as derived in appendix A. In the warmest regime, this limit provides an expression for the maximum value of M , whereas, in the intermediate regime, M exhibits a transient peak at a value greater than its long time limit.

It is also notable that the expression in (33) is independent of the initial conditions ΔD_{init} and h_0 . We therefore consider the limit in which the initial boundary layer depth goes to zero. In this case, the nondimensional time τ goes to infinity for any positive t , according to (18). The long time limit of the system is thereby reached immediately. Therefore, in the limit of an initially shallow boundary layer, the solution for M is given explicitly by the expression in (33).

The boundaries between each of the three regimes are given by

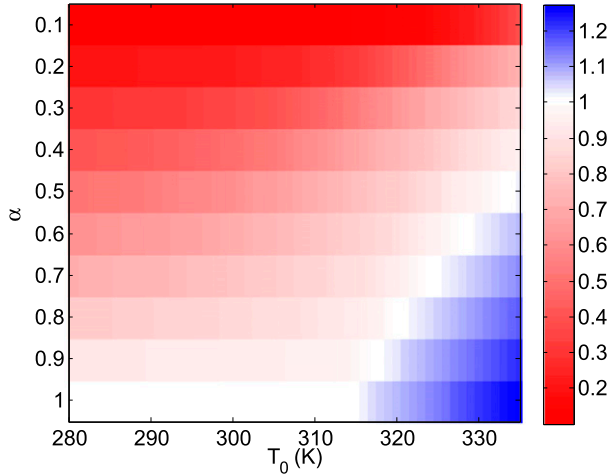


FIG. 4. Maximum relative humidity achieved at the top of the boundary layer during its evolution as a function of T_0 and α , for $h_0 = 100$, $v_{\text{sfc}} = 5 \text{ m s}^{-1}$, and $F_{\text{rad}} = 200 \text{ W m}^{-2}$.

$$\text{Peak: } q^*(T_0) < \frac{F_{\text{rad}}}{\alpha \rho C_T v_{\text{sfc}} L_v}, \quad (34)$$

$$\text{Intermediate: } \frac{F_{\text{rad}}}{\alpha \rho C_T v_{\text{sfc}} L_v} < q^*(T_0) < \left(\frac{1}{A_R} + \frac{1}{\alpha} \right) \frac{F_{\text{rad}}}{\rho C_T v_{\text{sfc}} L_v}, \quad \text{and} \quad (35)$$

$$\text{Asymptotic: } q^*(T_0) > \left(\frac{1}{A_R} + \frac{1}{\alpha} \right) \frac{F_{\text{rad}}}{\rho C_T v_{\text{sfc}} L_v}, \quad (36)$$

as derived in [appendix B](#). Increasing the initial atmospheric temperature T_0 , the evaporative fraction α , or the surface wind speed v_{sfc} ; or decreasing the net surface radiative input F_{rad} each has the effect of moving toward the asymptotic regime.

For most reasonable parameter choices, the boundary layer does not achieve saturation during its evolution, as shown in [Fig. 4](#). Supersaturations (in which the relative humidity at the top of the boundary layer exceeds 1) occur only at particularly high values of surface moisture and preinitial temperature. Since this model does not account for cloud formation in the boundary layer, it is ill equipped to handle supersaturations. However, for the majority of relevant parameter space, they do not occur.

4. Scaling of peak CAPE

By considering a parcel lifted from the boundary layer with moist static energy M into the free troposphere, whose environmental moist static energy is a constant D_0 in height and time, we calculate an approximate dimensional CAPE as a function of the boundary layer moist static energy surplus:

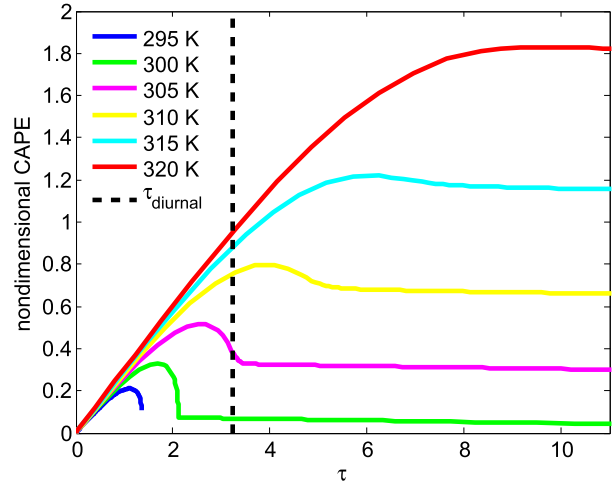


FIG. 5. Evolution of CAPE with time for several different values of T_0 , given $\alpha = 0.5$. Here, CAPE is nondimensionalized by a factor of $\rho C_T v_{\text{sfc}} F_{\text{rad}}^{-1}$, while time is nondimensionalized according to (18). The dashed black line displays the end of a 12-h diurnal time scale corresponding to the particular parameter choices $h_0 = 100 \text{ m}$ and $v_{\text{sfc}} = 5 \text{ m s}^{-1}$.

$$\text{CAPE} \approx (M - D_0) \ln \left(\frac{T_h}{T_{\text{LNB}}} \right), \quad (37)$$

where T_h is the temperature at the top of the boundary layer, and T_{LNB} is the temperature at the parcel's level of neutral buoyancy. It is assumed that the deep convection resulting from the stored CAPE will reach the tropopause and therefore that the temperature at the level of neutral buoyancy is coincident with the temperature at the tropopause in a typical column. Taking a rough average of data from [Hoinka \(1999\)](#), [Holton et al. \(1995\)](#), and the *U.S. Standard Atmosphere* ([COESA 1976](#)), we assume a value of $T_{\text{LNB}} \approx 220 \text{ K}$ for a midlatitude column.

[Figure 5](#) shows the time evolution of CAPE for several values of the preinitial near-surface air temperature T_0 , for a given choice of the surface moisture parameter. The functional forms of the time evolution of CAPE closely resemble those of the time evolution of μ , since CAPE in this model has a linear dependence on boundary layer moist static energy. However, CAPE also depends on the height of the boundary layer: as η increases with time, the top of the boundary layer becomes progressively colder. Most notably, in the asymptotic regime, η continues to grow linearly after δ goes to zero. In those cases, since the long time limit of D is D_0 , the entire column reverts to its preinitial dry adiabatic temperature profile. Therefore, as h increases linearly with time, T_h must decrease along a dry adiabat. Consequentially, while M remains at its asymptotic value for infinite time, CAPE actually decreases with time after the dry static energy surplus is sufficiently small.

Therefore, CAPE has a transient peak in every regime. This transience is due to the competing effects of two different mechanisms: Surface fluxes heat and moisten the boundary layer, thereby increasing the thermodynamic instability of the column. Meanwhile, the upward growth of the boundary layer engenders entrainment of dry air from the free troposphere above, acting to decrease instability. CAPE is further diminished as the increasing altitude of the boundary layer top lessens the area of positive buoyancy for lifted parcels. Near the beginning of this initial-value problem, the surface fluxes dominate as the boundary layer grows slowly, but they are eventually overwhelmed by the boundary layer growth process—this is the time at which peak CAPE is reached.

The value of peak CAPE increases monotonically with increasing temperature when other parameters are held fixed.

The functional relationship between peak CAPE and initial near-surface air temperature is shown by the solid green line in Fig. 6. For any given fixed set of parameters (F_{rad} , α , h_0 , and v_{sfc}), peak CAPE is found to increase approximately exponentially with increasing temperature T_0 . Note that dimensional CAPE in this model is considerably higher than that which is observed in nature; this is due to the idealizations made in constructing the model, in particular the assumption that the boundary layer is topped by a perfectly dry adiabatic layer with unlimited depth. The effect of this assumption is explored in Fig. 7, which shows the time evolution of the vertical temperature profile for an example solution at $T_0 = 305$ K. Figure 7c shows the most unstable temperature profile in the evolution of the column, under the assumption that the free troposphere follows the dry adiabatic lapse rate to an infinite height. In this case, CAPE is estimated by (37) to be $10\,600 \text{ J kg}^{-1}$. In Fig. 7d, however, the free troposphere is given a lapse rate more typical of the real atmosphere by relaxing that same most unstable profile to the *U.S. Standard Atmosphere* (COESA 1976) above the boundary layer. With this modification, an explicit level of neutral buoyancy exists, and CAPE is directly calculated to be 4500 J kg^{-1} , a value that more closely reflects levels of extreme CAPE that might be observed in a continental severe weather environment. While the magnitude of the peak of CAPE is significantly reduced by the implementation of a more realistic free troposphere, one would expect that the overall scaling of CAPE with T_0 would retain its functional form if this artificial correction were applied across the board.

Combining (33) and (37) provides an expression for CAPE as a function of the solution to the Clausius–

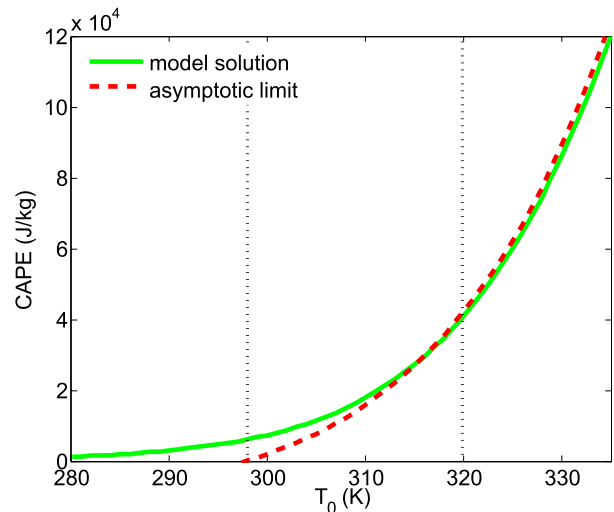


FIG. 6. Modeled dimensional peak CAPE as a function of T_0 (solid green line) for $\alpha = 0.5$, $h_0 = 100$ m, $v_{\text{sfc}} = 5 \text{ m s}^{-1}$, and $F_{\text{rad}} = 200 \text{ W m}^{-2}$; and a theoretical curve (dashed red line) corresponding to the asymptotic limit of CAPE that arises as $t \rightarrow \infty$, or $h_0 \rightarrow 0$. This curve is an exact solution to the Clausius–Clapeyron relation, as described by (38). The dotted black lines indicate the boundaries between the three regimes of model solutions.

Clapeyron equation relating saturation specific humidity to temperature:

$$\lim_{t \rightarrow \infty} \text{CAPE} = \left[L_v q^*(T_0) - \frac{F_{\text{rad}}}{\alpha \rho C_T v_{\text{sfc}}} \right] \ln \left(\frac{T_h}{T_{\text{LNB}}} \right). \quad (38)$$

This solution, shown by the dashed red line in Fig. 6, defines the response of the long time limit of CAPE to changes in temperature. It therefore corresponds exactly to peak CAPE in the asymptotic (warmest) regime for any initial boundary layer depth and in all regimes for the limit in which $h_0 \rightarrow 0$. The solution is linearly dependent on $q^*(T_0)$, and peak CAPE therefore scales exactly according to the Clausius–Clapeyron relation in the temperature space for which it applies.

As peak CAPE increases with increasing temperature, so too does the time required for peak CAPE to be achieved. This presents an issue, since in nature the boundary layer does not grow continuously for infinite time. Instead, energetic input to the system stops as the sun sets and the net radiative input to the surface goes to zero. This issue could be addressed by imposing a diurnal cycle on the surface radiative input; for simplicity, we merely introduce a limiting dimensional time scale after which the constant radiation is to be cut off. We assume a cutoff time scale of 12 h (or nondimensionally, $\tau_{\text{diurnal}} = C_T v_{\text{sfc}} h_0^{-1} \times 12 \text{ h}$) to be a duration representative of diurnal radiative input. The maximum dimensional CAPE achieved within time τ_{diurnal} is shown

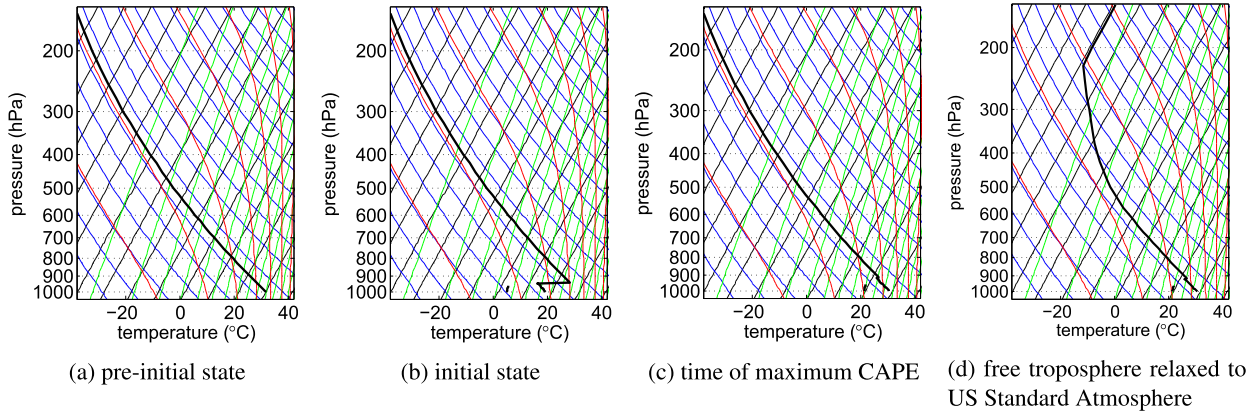


FIG. 7. Skew T diagrams depicting the vertical profile of temperature (solid black line) and dewpoint temperature (dashed black line) for an example model solution in which $T_0 = 305$ K, $\alpha = 0.5$, $h_0 = 500$ m, $v_{sfc} = 5$ m s $^{-1}$, and $F_{rad} = 200$ W m $^{-2}$, at (a) $t < 0$, (b) $t = 0$, (c) the time at which maximum CAPE is achieved, and (d) as in (c), but with the temperature of the free troposphere relaxed to that of the *U.S. Standard Atmosphere* (COESA 1976).

in Fig. 8 as a function of T_0 for a particular choice of h_0 , v_{sfc} , α , and F_{rad} .

The imposition of the diurnal time limit introduces a new behavior for peak CAPE values at high temperature. This model predicts that, for a given choice of constant parameters, increasing T_0 will cause the peak in CAPE to occur later in the day. At low temperatures (in this case, $T_0 \lesssim 305$ K), the CAPE peak occurs prior to the end of the diurnal time scale, so the curve of peak CAPE with T_0 retains its exponential nature. At higher temperatures, CAPE is still increasing when $\tau = \tau_{diurnal}$, so the maximum in CAPE occurs at the diurnal time limit. In this regime, the maximum in CAPE still increases with increasing T_0 , but its rate of increase is lessened. A consequence of this is the existence of a maximum in the sensitivity of peak CAPE with respect to temperature. In Fig. 8, this sensitivity maximum occurs at $T_0 \approx 305$ K.

Finally, we vary the surface moisture α , wind speed v_{sfc} , and initial boundary layer height h_0 parameters to determine their effects on peak CAPE. These results are shown in Fig. 9. The flux of moist static energy from the surface to the boundary layer that fuels CAPE buildup is a function of both surface moisture and wind speed. Increasing either the surface moisture parameter or the surface wind speed parameter has the effect of modifying the Bowen ratio such that a greater portion of the surface moist static energy flux is partitioned to latent heat flux. Both peak CAPE and the time taken to achieve it are thereby increased. As a consequence, CAPE increases more quickly with increasing temperature, but the regime of maximum sensitivity is shifted to lower temperatures. Nevertheless, for a fixed T_0 , increasing either α or v_{sfc} has the monotonic effect of increasing peak CAPE.

The exception is that, for sufficiently high temperatures (in this example, $T_0 \gtrsim 320$ K), increasing α slightly decreases the maximum CAPE that can be achieved within the diurnal time scale. This is due to the assumption that a moister surface is associated with a moister and therefore cooler initial boundary layer. This effect acts to decrease the initial Bowen ratio, thereby increasing the time taken for peak CAPE to be reached. Imposing the diurnal time cutoff translates this slower CAPE buildup into a smaller value of maximum CAPE achieved within that time.

At low T_0 , changing h_0 has little effect on peak CAPE. However, a deeper boundary layer requires a larger total flux to achieve an equivalent buildup of moist static

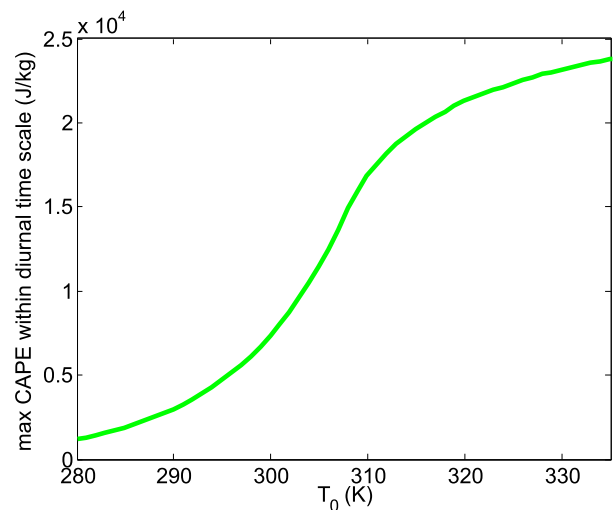


FIG. 8. Modeled maximum CAPE within a diurnal time scale, as a function of T_0 for $\alpha = 0.5$, $h_0 = 100$ m, $v_{sfc} = 5$ m s $^{-1}$, and $F_{rad} = 200$ W m $^{-2}$.

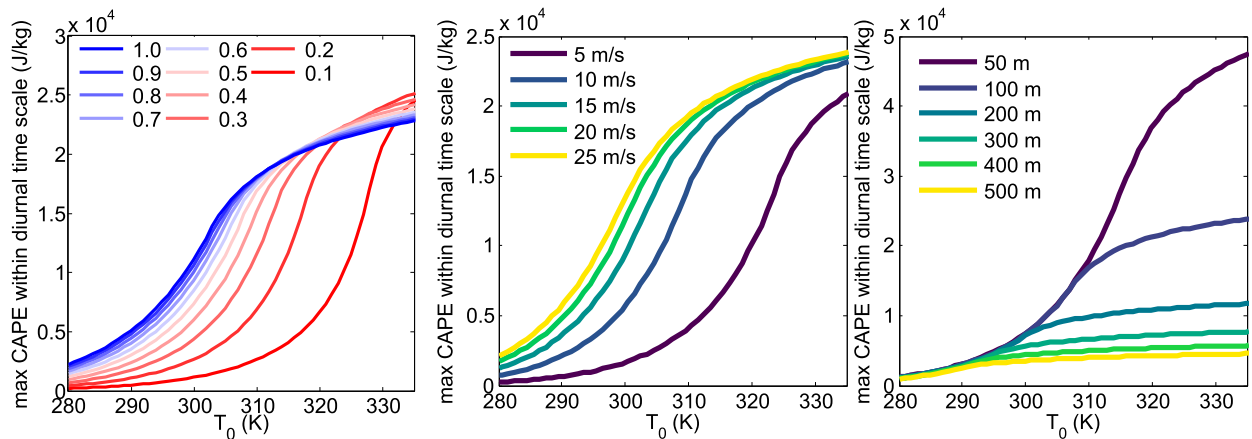


FIG. 9. Modeled maximum CAPE within a diurnal time scale, as a function of T_0 with varying α , v_{sfc} , and h_0 .

energy. Raising the initial boundary layer height thereby has the effect of prolonging the time needed for peak CAPE to be achieved. The temperature at which the diurnal cutoff time scale becomes the limiting factor for peak CAPE is therefore lower for solutions with deeper boundary layers. Thus, while the diurnal cutoff time is unimportant at sufficiently cool temperatures, increasing h_0 monotonically decreases the maximum CAPE within the diurnal time scale at warmer temperatures.

5. Discussion

The idealized column model developed here introduces a theoretical constraint on transient peak CAPE for a particular mechanism of instability generation unique to continental severe weather environments. Both in the presence and in the absence of a limiting time scale, the model predicts increasing peak CAPE with the increasing temperature of the preinitial dry column that provides the capping inversion.

In the case of no limiting time scale, peak CAPE scales exponentially with the temperature of the elevated dry layer and follows an exact solution to the Clausius–Clapeyron equation. For a given range of temperatures, the magnitude of peak CAPE is a direct function of the preinitial saturation specific humidity of the dry column. This is consistent with past studies linking the growth rate of CAPE with temperature to the increase in the water vapor capacity of air with increasing temperature [as found by Romps (2011) for tropical climate]. The idealized column model derived here extends this theoretical thermodynamic constraint on severe convection to continental environments.

In the case in which radiative input to the surface is limited by the time scale of the diurnal cycle, peak

CAPE also increases monotonically with dry-layer temperature, but, as temperature increases, the peak occurs at a later time. This result is consistent with Gensini and Mote (2015), which found a delay in the diurnal distribution of severe convection in dynamically downscaled future climate simulations. At sufficiently high temperatures, the time of peak CAPE coincides with the end of the diurnal time scale, at which point the relationship between temperature and peak CAPE diverges from the exponential Clausius–Clapeyron scaling.

Finally, we conclude that high temperature, high available moisture in the land surface, and high surface winds are each conducive to increased peak CAPE. This suggests that, for the particular means of CAPE buildup studied by this model, increasingly severe continental convection would be permitted in warmer climates, should other environmental parameters be unchanged. This result could also be extended to seasonal variability of severe convection, with wetter winter or spring seasons possibly yielding moister soils that would be conducive to higher peak CAPE conditions. Future studies could seek to identify such correlations in the observational record.

Care should be taken not to overgeneralize these results. No determinations are made about changes in deep-layer shear or convective initiation, both of which are important for supporting severe convection over land. However, this model does provide a theoretically based constraint on the magnitude of CAPE that can arise through diabatic heating in typical continental severe storm environments.

Acknowledgments. We thank Howard Bluestein, Paul O’Gorman, and Earle Williams for their helpful comments over the course of this research. We also thank three anonymous reviewers for their constructive feedback on the

manuscript. Financial support was provided by the Office of Naval Research through Award N00014-14-1-0062.

APPENDIX A

Derivation of Long Time Moist Static Energy Limit in Asymptotic Regime

We begin with the nondimensional equation governing the flux of moist static energy from the surface into the boundary layer [i.e., (29)]:

$$(1 - \alpha)(\delta + \delta_s) + \alpha(\mu_s - \mu) - 1 = \Phi. \quad (\text{A1})$$

In the limit of infinite time ($\tau \rightarrow \infty$), the dry static energy deficit δ goes to 0, while the surface dry static energy δ_s goes to 1 (as $T_{\text{sfc}} \rightarrow T_0$). Therefore, applying the infinite time limit to this equation yields

$$(1 - \alpha) + \alpha \lim_{\tau \rightarrow \infty} (\mu_s - \mu) - 1 = \Phi. \quad (\text{A2})$$

Rearranging and redimensionalizing gives

$$\lim_{t \rightarrow \infty} [M - D_0 - c_p T_{\text{sfc}} - L_v q^*(T_{\text{sfc}})] = -\frac{F_{\text{rad}}}{\alpha \rho C_T v_{\text{sfc}}} - D_0. \quad (\text{A3})$$

We now substitute $\lim_{t \rightarrow \infty} T_{\text{sfc}} = T_0$ and $c_p T_0 = D_0$ to yield

$$\lim_{t \rightarrow \infty} M - D_0 = L_v q^*(T_0) - \frac{F_{\text{rad}}}{\alpha \rho C_T v_{\text{sfc}}}. \quad (\text{A4})$$

APPENDIX B

Derivation of Regime Boundaries

The boundaries between the peak, intermediate, and asymptotic regimes are derived in terms of the long time limits of model variables.

In the intermediate and asymptotic regimes, the long time limit of moist static energy M is given by (33), as derived in appendix A:

$$\lim_{t \rightarrow \infty} M - D_0 = L_v q^*(T_0) - \frac{F_{\text{rad}}}{\alpha \rho C_T v_{\text{sfc}}}. \quad (\text{B1})$$

When the long time limit of the moist static energy surplus is positive ($\lim_{t \rightarrow \infty} M - D_0 > 0$), the system is in either the intermediate or asymptotic regime. Therefore, when the limit is negative ($\lim_{t \rightarrow \infty} M - D_0 < 0$), the system must be in the peak regime. Substituting this inequality into the above equation and rearranging yields the condition

$$q^*(T_0) < \frac{F_{\text{rad}}}{\alpha \rho C_T v_{\text{sfc}} L_v} \quad (\text{B2})$$

for the peak regime.

To distinguish between the intermediate and fully asymptotic regimes, we start from the nondimensional equation for the time rate of change of the moist static energy surplus [i.e., (23)]:

$$\frac{d\mu}{d\tau} = \frac{\Phi}{\eta} - \frac{\mu A_R}{\eta \delta} (\delta_s + \delta - 1). \quad (\text{B3})$$

In the fully asymptotic regime, the moist static energy surplus μ increases asymptotically toward its long time limit for all time and does not exhibit a transient peak. Therefore, the time derivative of μ is positive-definite:

$$\frac{d\mu}{d\tau} = \frac{\Phi}{\eta} - \frac{\mu A_R}{\eta \delta} (\delta_s + \delta - 1) > 0. \quad (\text{B4})$$

Simplifying and rearranging yields

$$\Phi > \mu A_R \left(\frac{\delta_s + \delta - 1}{\delta} \right). \quad (\text{B5})$$

We now take the long time limit of this inequality:

$$\Phi > \left(\lim_{\tau \rightarrow \infty} \mu \right) A_R \lim_{\tau \rightarrow \infty} \left(\frac{\delta_s + \delta - 1}{\delta} \right). \quad (\text{B6})$$

Since $\lim_{\tau \rightarrow \infty} \delta_s = 1$, it can be shown that

$$\lim_{\tau \rightarrow \infty} \left(\frac{\delta_s + \delta - 1}{\delta} \right) = 1. \quad (\text{B7})$$

Substituting this into (B6) and redimensionalizing yields

$$\frac{F_{\text{rad}}}{\rho C_T v_{\text{sfc}}} > A_R \lim_{t \rightarrow \infty} M - D_0. \quad (\text{B8})$$

We now substitute the long time limit of moist static energy ($\lim_{t \rightarrow \infty} M$) from (33) into the above inequality, resulting in the condition

$$q^*(T_0) > \left(\frac{1}{A_R} + \frac{1}{\alpha} \right) \frac{F_{\text{rad}}}{\rho C_T v_{\text{sfc}} L_v} \quad (\text{B9})$$

for the asymptotic regime.

The intermediate regime exists for the range of $q^*(T_0)$ between the peak and asymptotic regimes:

$$\frac{F_{\text{rad}}}{\alpha \rho C_T v_{\text{sfc}} L_v} < q^*(T_0) < \left(\frac{1}{A_R} + \frac{1}{\alpha} \right) \frac{F_{\text{rad}}}{\rho C_T v_{\text{sfc}} L_v}. \quad (\text{B10})$$

REFERENCES

- Bluestein, H. B., 2007: Advances in applications of the physics of fluids to severe weather systems. *Rep. Prog. Phys.*, **70**, 1259–1323, doi:10.1088/0034-4885/70/8/R01.
- Brooks, H. E., 2009: Proximity soundings for severe convection for Europe and the United States from reanalysis data. *Atmos. Res.*, **93**, 546–553, doi:10.1016/j.atmosres.2008.10.005.
- , 2013: Severe thunderstorms and climate change. *Atmos. Res.*, **123**, 129–138, doi:10.1016/j.atmosres.2012.04.002.
- , C. A. Doswell III, and M. P. Kay, 2003a: Climatological estimates of local daily tornado probability for the United States. *Wea. Forecasting*, **18**, 626–640, doi:10.1175/1520-0434(2003)018<0626:CEOLDT>2.0.CO;2.
- , J. W. Lee, and J. P. Craven, 2003b: The spatial distribution of severe thunderstorm and tornado environments from global reanalysis data. *Atmos. Res.*, **67–68**, 73–94, doi:10.1016/S0169-8095(03)00045-0.
- COESA, 1976: *U.S. Standard Atmosphere, 1976*. NOAA, 227 pp.
- Del Genio, A. D., M.-S. Yao, and J. Jonas, 2007: Will moist convection be stronger in a warmer climate? *Geophys. Res. Lett.*, **34**, L16703, doi:10.1029/2007GL030525.
- Diffenbaugh, N. S., M. Scherer, and R. J. Trapp, 2013: Robust increases in severe thunderstorm environments in response to greenhouse forcing. *Proc. Natl. Acad. Sci. USA*, **110**, 16 361–16 366, doi:10.1073/pnas.1307758110.
- Doswell, C. A., III, H. E. Brooks, and R. A. Maddox, 1996: Flash flood forecasting: An ingredients-based methodology. *Wea. Forecasting*, **11**, 560–581, doi:10.1175/1520-0434(1996)011<0560:FFFAIB>2.0.CO;2.
- Emanuel, K. A., 1994: *Atmospheric Convection*. Oxford University Press, 580 pp.
- Gensini, V. A., and T. L. Mote, 2015: Downscaled estimates of late 21st century severe weather from CCSM3. *Climatic Change*, **129**, 307–321, doi:10.1007/s10584-014-1320-z.
- Grams, J. S., R. L. Thompson, D. V. Snively, J. A. Prentice, G. M. Hodges, and L. J. Reames, 2012: A climatology and comparison of parameters for significant tornado events in the United States. *Wea. Forecasting*, **27**, 106–123, doi:10.1175/WAF-D-11-00008.1.
- Hoinka, K. P., 1999: Temperature, humidity, and wind at the global tropopause. *Mon. Wea. Rev.*, **127**, 2248–2265, doi:10.1175/1520-0493(1999)127<2248:THAWAT>2.0.CO;2.
- Holton, J. R., 2004: *An Introduction to Dynamic Meteorology*. 4th ed. Elsevier, 535 pp.
- , P. H. Haynes, M. E. McIntyre, A. R. Douglass, R. B. Rood, and L. Pfister, 1995: Stratosphere–troposphere exchange. *Rev. Geophys.*, **33**, 403–439, doi:10.1029/95RG02097.
- Lilly, D. K., 1968: Models of cloud-topped mixed layers under a strong inversion. *Quart. J. Roy. Meteor. Soc.*, **94**, 292–309, doi:10.1002/qj.49709440106.
- Monin, A., and A. Obukhov, 1954: Basic laws of turbulent mixing in the surface layer of the atmosphere. *Tr. Geofiz. Inst., Akad. Nauk SSSR*, **151**, 163–187.
- Parodi, A., and K. Emanuel, 2009: A theory for buoyancy and velocity scales in deep moist convection. *J. Atmos. Sci.*, **66**, 3449–3463, doi:10.1175/2009JAS3103.1.
- Rasmussen, E. N., and D. O. Blanchard, 1998: A baseline climatology of sounding-derived supercell and tornado forecast parameters. *Wea. Forecasting*, **13**, 1148–1164, doi:10.1175/1520-0434(1998)013<1148:ABCOSD>2.0.CO;2.
- Romps, D. M., 2011: Response of tropical precipitation to global warming. *J. Atmos. Sci.*, **68**, 123–138, doi:10.1175/2010JAS3542.1.
- Schultz, D. M., Y. P. Richardson, P. M. Markowski, and C. A. Doswell III, 2014: Tornadoes in the central United States and the clash of air masses. *Bull. Amer. Meteor. Soc.*, **95**, 1704–1712, doi:10.1175/BAMS-D-13-00252.1.
- Seeley, J. T., and D. M. Romps, 2015: The effect of global warming on severe thunderstorms in the United States. *J. Climate*, **28**, 2443–2458, doi:10.1175/JCLI-D-14-00382.1.
- Singh, M. S., and P. A. O’Gorman, 2013: Influence of entrainment on the thermal stratification in simulations of radiative-convective equilibrium. *Geophys. Res. Lett.*, **40**, 4398–4403, doi:10.1002/grl.50796.
- Sobel, A. H., and S. J. Camargo, 2011: Projected future seasonal changes in tropical summer climate. *J. Climate*, **24**, 473–487, doi:10.1175/2010JCLI3748.1.
- Tippett, M. K., J. T. Allen, V. A. Gensini, and H. E. Brooks, 2015: Climate and hazardous convective weather. *Curr. Climate Change Rep.*, **1**, 60–73, doi:10.1007/s40641-015-0006-6.
- Trapp, R. J., and K. A. Hoogewind, 2016: The realization of extreme tornadic storm events under future anthropogenic climate change. *J. Climate*, **29**, 5251–5265, doi:10.1175/JCLI-D-15-0623.1.
- , N. S. Diffenbaugh, H. E. Brooks, M. E. Baldwin, E. D. Robinson, and J. S. Pal, 2007: Changes in severe thunderstorm environment frequency during the 21st century caused by anthropogenically enhanced global radiative forcing. *Proc. Natl. Acad. Sci. USA*, **104**, 19 719–19 723, doi:10.1073/pnas.0705494104.
- Weisman, M. L., and J. B. Klemp, 1982: The dependence of numerically simulated convective storms on vertical wind shear and buoyancy. *Mon. Wea. Rev.*, **110**, 504–520, doi:10.1175/1520-0493(1982)110<0504:TDonSC>2.0.CO;2.
- Zipser, E. J., D. J. Cecil, C. Liu, S. W. Nesbitt, and D. P. Yorty, 2006: Where are the most intense thunderstorms on Earth? *Bull. Amer. Meteor. Soc.*, **87**, 1057–1071, doi:10.1175/BAMS-87-8-1057.